UCID- 17935

Lawrence Livermore Laboratory

PERFORMANCE MODEL FOR A CCTV-MTI

MASTER

D. P. Dunn
D. L. Dunbar

September 20, 1978

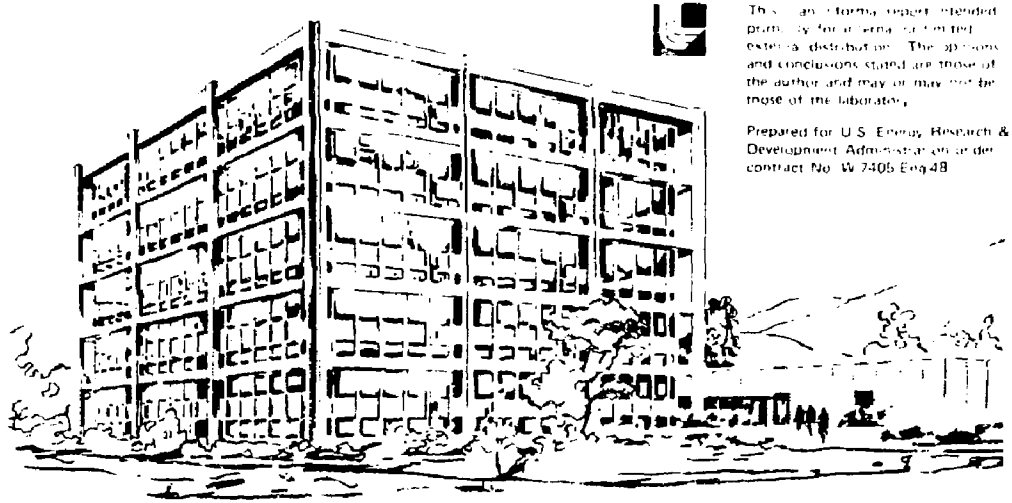

Prepared for U.S. Energy Research & Development Administration under contract No. W-7405-Eng-48

CONTENTS

ABSTRACT

CCTV-MTI (closed circuit television - moving target indicator) monitors represent typical components of access control systems, as for example in a material control and accounting (MC&A) safeguards system. This report describes a performance model for a CCTV-MTI monitor. The performance of a human in an MTI role is a separate problem and is not addressed here. This work was done in conjunction with the NRC sponsored LLL assessment procedure for MC&A systems which is presently under development.

We develop a noise model for a generic camera system and a model for the detection mechanism for a postulated MTI design. These models are then translated into an overall performance model. Measures of performance are probabilities of detection and false alarm as a function of intruder-induced grey level changes in the protected area. Sensor responsivity, lens F-number, source illumination and spectral response were treated as design parameters.

Some specific results are illustrated for a postulated design employing a camera with a Si-target vidicon. Reflectance or light level changes in excess of 10% due to an intruder will be detected with a very high probability for the portion of the visible spectrum with wavelengths above 500 nm. The resulting false alarm rate was less than one per year.

We did not address sources of nuisance alarms due to adverse environments, reliability, resistance to tampering, nor did we examine the effects of the spatial frequency response of the optics. All of these are important and will influence overall system detection performance.

This report was prepared as an account of work sponsored by the U.S. Nuclear Regulatory Commission, under the auspices of the U.S. Department of Energy Contract No. W-7405-ENG-48.

PERFORMANCE MODEL FOR A CCTV-MTI

Introduction

Closed circuit television - moving target indicator (CCTV-MTI) instruments are used for access control in numerous industrial-commercial applications. One such application is in material control and accounting systems for nuclear fuel processing facilities. LLL is involved in a program of work for the NRC which is directed toward developing a methodology for accessing the effectiveness of MC & A systems [1,2]. The methodology requires many types of mathematical models including performance models for security instruments.

A performance model for a CCTV-MTI design is developed herein which illustrates probabilities of detection in terms of changes in scene reflectance for various wavelengths of scene illumination. The performance model is a function of the detection scheme and of the underlying statistical variations in the signal due to quantum noise and electronic preamplifier noise.

We are strictly concerned with characterizing the performance of an electronic MTI design as opposed to evaluating the performance of a human as a moving target detector.

A block diagram for a CCTV-MTI system is shown in Figure 1. The MTI processor can be of several different designs [3,4]. One approach uses sensors, placed on the face of a monitor, to detect movement by sensing light changes in sensitive areas (e.g., suction cups which contain light-sensitive diodes to detect changes in light patterns). This design requires a video monitor. A second type looks for changes in the energy spectrum of the video signal [5,6]. Another type senses changes in the video signal of several hundred pixels* between fields or frames (two fields equal one video frame) [7,8]. The latter two types do not require a video monitor.

---

*A pixel is a picture element on a TV raster.

In all cases the objective is to detect gray contrast changes in the video information due to target induced nonstationary conditions. The problem is a probabilistic one due to the statistical variations in the video signal. A simplified block diagram of a MTI processor of the third type mentioned above is shown in Figure 2. A performance analysis will be done using this design concept. The analysis is applicable to other CCTV-MTI designs.

Noise Considerations

The statistical variations in the video signal for the system shown in Figures 1 and 2 can be attributed primarily to the early electronics which in this case is the preamplifier and sensor of the camera. We will assume that subsequent amplification will contribute very little to the overall degradation of the video information. Generally two sources of signal variation are present [9-10]. One is quantum noise (photon-limited statistics) where the signal is characterized by low photo-electron generation rates. A second source is additive circuit noise which is generated by both active and passive electronic components. The principal consituents in this case are thermal and shot noise. Thermal noise (also called Johnson noise or white noise) exists in all resistors and has a wideband spectrum. Shot noise is due to erratic movement of charge carriers in active devices (transistors and diodes) and also has a wideband spectrum.

Figure 3 depicts the signal path of a camera and is representative of numerous camera designs. The primary noise sources for the early electronics are shown in Figure 4 and are defined as:

$$\overline{I}_{sig}^2 = 2e\, I_{savg} \left(\frac{amp^2}{Hz}\right) \text{ shot noise in detector (light sensor)}$$

$$\overline{I}_{D}^2 = 2e\, I_{D} \left(\frac{amp^2}{Hz}\right) \text{ shot noise in detector due to dark current} \quad (1)$$

$$\overline{I}_{ng}^2 = \frac{4kT}{R_g} \left(\frac{amp^2}{Hz}\right) \text{ thermal noise in source resistor } R_g$$

$$\overline{I}_{nf}^2 = \frac{4kT}{R_f}\left(\frac{amp^2}{Hz}\right) \quad \text{thermal noise in feedback resistor } R_f$$

$$\overline{I}_{np}^2 = \frac{4kT}{R_{np}}\left(\frac{amp^2}{Hz}\right) \quad \text{parallel noise contribution of amplifier} \quad (1) \text{ con't}$$

$$\overline{V}_{ns}^2 = 4kT\, R_{ns}\left(\frac{V^2}{Hz}\right) \quad \text{series noise contribution of amplifier}$$

where

e = charge on an electron (1.59×10^{-19} coulomb),

I_{savg} = average value of signal current from sensor,

I_D = dark current in sensor,

k = Boltzman's constant (1.38×10^{-23} J/°k),

T = temperature in Kelvin degrees.

Furthermore, R_{np} and R_{ns} are equivalent parallel and series noise resistors which represent contributions due to both shot noise and thermal noise internal to the amplifier. Using this approach allows us to analyze a generic class of preamplifier designs.

As a result of introducing the noise sources in Figure 4, the R-C components and the amplifiers can be considered to be noise free. Therefore, the voltage gain of the preamplifier per se will be modeled as having a single time constant $\tau_a = 1/\omega_a$ and a dc-voltage gain K_d:

$$\frac{V_{o1}}{V_\epsilon} \triangleq \frac{K_d}{j\omega/\omega_a + 1}$$

where ω is frequency in radians and $j = \sqrt{-1}$. We will further assume that secondary amplification is wideband with a closed-loop dc voltage gain denoted A_2^{cl}.

The output mean-square noise voltage $\overline{V}_o^2(\omega)$ in volts-squared per hertz due to each of the noise sources in Figure 4 can be obtained by using the superposition theorem of circuit theory:

$$\overline{V}_o^2(\omega) = \overline{V}_o^2(\overline{I}_{sig},\omega) + \overline{V}_o^2(\overline{I}_D,\omega) + \overline{V}_o^2(\overline{I}_{ng},\omega) + \overline{V}_o^2(\overline{I}_{np},\omega)$$

$$+ \overline{V}_o^2(\overline{I}_{nf},\omega) + \overline{V}_o^2(\overline{V}_{ns},\omega) \quad \left(\frac{V^2}{Hz}\right) \qquad (2)$$

where $\overline{V}_o^2(x,\omega)$ denotes the output contribution due to the noise source x as a function of frequency ω. Derivations for each of the components in (2) are provided in Appendix A. Using these results, the mean-square noise voltage can be expressed as:

$$\overline{V}_o^2(\omega) = \left|A_1^{cl} A_2^{cl}\right|^2 \left[|H_1(\omega)|^2 R_g^2 \left(\overline{I}_{sig}^2 + \overline{I}_D^2 + \overline{I}_{ng}^2 + \overline{I}_{np}^2 + \overline{I}_{nf}^2\right) + |H_2(\omega)|^2 \left(\frac{R_f + R_g}{R_f}\right)^2 \cdot \overline{V}_{ns}^2\right] \qquad \left(\frac{V^2}{Hz}\right) \tag{3}$$

where

$$|H_1(\omega)|^2 \triangleq \frac{\omega_o^4}{\omega_o^4 - 2(1-2\rho^2)\omega_o^2\omega^2 + \omega^4} \tag{4}$$

$$|H_2(\omega)|^2 \triangleq \frac{\left(\frac{\omega_o^2}{\omega_b}\right)^2 (\omega_b + \omega)^2}{\omega_o^4 - 2(1-2\rho^2)\omega_o^2\omega^2 + \omega^4} \tag{5}$$

$\omega_o^2 \triangleq (\omega_a \cdot \omega_b)(1 + \beta A_1^{ol})$, (natural frequency, radians)

$\omega_b \triangleq \frac{R_f R_g}{R_f + R_g} C$ (radians)

$\rho \triangleq \frac{\omega_a + \omega_b}{2\omega_o}$ (damping coefficient)

$\beta \triangleq R_g/R_f$ (preamplifier feedback ratio)

$A_1^{ol} \triangleq \frac{K_d R_f}{R_g + R_f}$ (preamplifier open-loop dc voltage gain)

$$A_1^{Cl} \triangleq \frac{A_1^{Ol}}{1 + \beta A_1^{Ol}} \qquad \text{(preamplifier closed-loop dc voltage gain)}$$

$$A_2^{Cl} \triangleq \frac{V_o}{V_{o1}} \qquad \text{(2nd amplifier closed-loop dc voltage gain)}$$

The output noise voltage spectrum is illustrated in Figure 5. To obtain the output mean-square noise voltage the spectrum as given by (3) must be integrated over all frequencies. The integration is performed in Appendix A for $\rho^2 = 1/2$ which is representative of a typical design and the result is:

$$\overline{V}_o^2 = \frac{\pi}{2\sqrt{2}} f_o \left| A_1^{Cl} \cdot A^{Cl} \right|^2 \left\{ R_g^2 \left(\overline{I}_{sig}^2 + \overline{I}_D^2 + \overline{I}_{ng}^2 + \overline{I}_{np}^2 \right.\right.$$

$$\left.\left. + \overline{I}_{nf}^2 + \frac{1}{R_{eq}^2} \overline{V}_{ns}^2 \right) \right\} \qquad (V^2) \qquad (6a)$$

$$= \frac{\pi}{2\sqrt{2}} f_o \left| A_1^{Cl} \cdot A_2^{Cl} \right|^2 \left[R_g^2 \right] \left\{ 2e(I_{savg} + I_D) + \right.$$

$$\left. 4KT \left(\frac{1}{R_g} + \frac{1}{R_{np}} + \frac{1}{R_f} + \frac{R_{ns}}{R_{eq}^2} \right) \right\} \qquad (V^2) \qquad (6b)$$

where use was made of (1), $\omega_o = 2\pi f_o$, and where

$$R_{eq} \triangleq \frac{1}{2\pi f_o C}$$

In practice one normally finds that $\overline{I}_{sig}^2$ is small compared to the other noise sources and that $\overline{I}_{nf}^2$ and/or $\overline{V}_{ns}^2$ usually dominate. Equation (6) gives the variance of the output noise signal in terms of circuit parameters (for $\rho^2 = 1/2$) and can be used to compute input signal-to-noise ratio (SNR).

Detection Scheme

The video information from the camera is input to a MTI processor which employs a detection scheme to ascertain if contrast changes have occurred in the camera's field-of-view. A MTI design which is similar to one which has been employed commercially under the name Telesentry [7,8] will be used to illustrate detection performance modeling. The detection scheme looks at consecutive samples from an array of sensor points* in the video frame to determine if there have been contrast changes which are statistically significant.

The sample points on a video frame are staggered with greater concentrations at the top of the field-of-view (for far field detection) than for the other portions of the picture. The concentration at the top is such that if a uniform distribution did exist there would be a total of 1352 sample points. Instead there is a nonuniform distribution totaling 676 sample points. In contrast there are about 300,000 pixels in a standard T.V. picture.

A precursor alarm is set if a contrast change greater than a threshold occurs for any one sample point and for any other sample point within eight lines of the first for a field of video. An alarm is generated if a similar condition exists for the second field of video. The threshold in this case is two ADC** bits which is equal to 62.5 mV.

Based upon the noise analysis of the previous section, the video information from the camera for one pixel can be modeled as signal plus additive Gaussian noise, denoted s(i) with mean $\mu(i)$ and variance σ_s^2 and where i is discrete time.*** The detection mechanism looks for changes in s(i) at times i-1 and i. Therefore, define a contrast signal as:

$$\Delta s(i) = s(i)-s(i-1) \tag{7}$$

---

* The sensor points will be referred to as pixel sensors or pixel detectors.

** Analog-to-digital converter.

***The variance σ_s^2 is V_o^2 from (6).

with mean $\Delta\mu(i)$ and variance (assuming independence)

$$\sigma^2 = 2\sigma_s^2 \tag{8}$$

We can now establish two hypotheses for each pixel sensor: one where $\Delta s(i)$ is due to noise alone (H_0), and one where $\Delta s(i)$ is due to target induced gray contrast changes plus noise (H_1). These can be expressed as:

$$H_0: \quad \Delta s(i) = N(\Delta\mu_0, \sigma^2) \qquad \text{(Noise)}$$

$$H_1: \quad \Delta s(i) = N(\Delta\mu_1, \sigma^2) \qquad \text{(Signal plus noise)}$$

where $N(\Delta\mu, \sigma^2)$ denotes a Gaussian probability density function with mean $\Delta\mu$ and variance σ^2. Without loss of generality we can take $\Delta\mu_0 = 0$ and $\Delta\mu_1 = \Delta\mu$. The probability density functions are illustrated in Figure 6 along with two thresholds.

If $\Delta s(i)$ lies between $\pm\delta_T$ then H_0 is assumed to be correct, otherwise an H_1 condition is taken. We can express this situation in terms of a false alarm probability (P_{fa}) and a detection probability (P_d) given by:

$$P_{fa} = \text{Prob}\{|\Delta s(i)| > |\delta_T|, \text{ given that } H_0 \text{ is true}\}$$

$$= \frac{2}{\sqrt{2\pi}} \int_{\frac{\delta_T}{\sigma}}^{\infty} \exp\frac{\alpha^2}{2} \, d\alpha \tag{9}$$

$$P_d = \text{Prob}\{|\Delta s(i)| > |\delta_T|, \text{ given that } H_1 \text{ is true}\}$$

$$= \frac{1}{\sqrt{2\pi}} \int_{\frac{\delta_T - |\Delta\mu|}{\sigma}}^{\infty} \exp\frac{\alpha^2}{2} \, d\alpha \tag{10}$$

where these probabilities refer to the detection performance for a single pixel sensor/detector.

The performance for the system will not only depend upon the performance of the individual pixel detectors, but it is also a function of the number of pixel detectors involved. Detection will be enhanced if an event in the

camera's field-of-view caused a contrast change to occur on all of the individual pixel detectors. As a result, we will first consider a bounding case (lowest probability of detection and highest false-alarm probability) for a performance model.

The lowest detection probability of an event is achieved when only two spatially related pixel detectors experience a contrast change between times i-1 and i for each video field. The probability of detection for two pixel detectors in one field for a contrast of Δu is P_d^2 and represents the probability of getting a precursor alarm. P_d is given by (10). The probability that four pixel detectors (two in each field) will detect an event of contrast Δu is

$$P_D \triangleq P_d^4 \tag{11}$$

which represents a lower bound on the overall detection probability and is a function of the threshold δ_T.

The detection probability P_D will be increased if additional pixel detectors are involved. Assuming that n-number of pixel sensors within a spatial group of a field experience equal contrast changes, then the probability of obtaining a precursor alarm is:

$$P_{df} \triangleq 1-(1-P_d^2)^m$$

where m is obtained from a combinatorial formula

$$m \triangleq \frac{n!}{2!(n-2)!} \tag{12}$$

and is the combination of n things taken two at a time. An alarm will be signaled only if detection occurs in two successive video fields. Therefore, the overall detection probability is given by:

$$P_D = P_{df}^2$$

$$= [1 - (1-P_d^2)^m]^2 \tag{13}$$

For n = 2, m = 1 and (13) reduces to (11).

The highest false alarm probability occurs due to contributions from all of the pixel detectors and is a function of their spatial arrangement. The maximum density is approximately 21 pixel detectors for eight lines of video field whereas the average is about 10. Furthermore, there are 518 groups* of eight spatially related lines per frame. Each of these groups will influence the false alarm rate.

In calculating an upper bound, the maximum density of 21 pixel detectors per group will be used. A false alarm precursor condition will result for a group of spatially related detectors if any two of the 21 give false-alarms; furthermore, the corresponding probability is P_{fa}^2 where P_{fa} is given by (9). The probability of not receiving a false alarm from a group can be computed by

$$(1 - P_{fa}^2)^m$$

where m is obtained from the combinatorial formula in (12) and for n = 21, m = 210. But there are 259 groups per field. Therefore, the probability of not obtaining a false alarm precursor condition for the groups in a field is

$$(1 - P_{fa}^2)^{259 \cdot m}$$

The probability of not receiving a false alarm for a frame is therefore

$$\bar{P}_{FA} \triangleq [(1-P_{fa}^2)^{259 \cdot m}]^2$$

$$\approx (1 - P_{fa}^2)^{10^5}$$

---

*525 lines - 8 lines/group + 1 = 518 groups per frame or 259 groups per field.

where the above value of m was used. The resulting overall probability of false alarm is given by

$$P_{FA} = 1 - \bar{P}_{FA} = 1 - (1 - P_{fa}^2)^{10^5} \qquad (14)$$

P_{FA} is given approximately by

$$P_{FA} \approx 10^5 \cdot P_{fa}^2$$

for extremely small values of P_{fa}^2 which is determined by the variance σ^2 and by the threshold ϕ_T.

Equations (11) and (14) provide bounds on a performance model for the detection scheme described above.

Performance Characterization

To illustrate the performance characterization for the design concept described in the previous section a value for the variance $\sigma^2 = 2\sigma_s^2$ in (8) must be obtained. Instead of analyzing a specific camera design along the lines of the noise analysis given previously, we will obtain an approximate σ_s^2 using typical parameter values.

The SNR can be expressed as

$$SNR = \frac{I_s^2}{\bar{I}_{in}^2} = \frac{V_o^2}{\sigma_s^2}$$

where I_s is input signal current, $\bar{I}_{in}^2$ is equivalent input noise current, and $\bar{I}_{in}^2$ and σ_s^2 are related by Eq. (A-19). A typical camera output SNR is 45 db for 1 V p-p into 75 ohms and is representative of an $\bar{I}_{in}$ of 5 nA or a $\bar{V}_o^2$ equal to:

$$\sigma_s^2 = 3.16 \times 10^{-5} \quad V^2$$

The variance σ^2 describing the detector is $2\sigma_s^2$ from (8). Therefore,

$$\sigma = 7.95 \text{ mV} \tag{15}$$

The threshold value was given previously as

$$\delta_T = 62.5 \text{ mV}$$

so that

$$\frac{\delta_T}{\sigma} = 7.86$$

which suggests that a very low P_{fa} should result.

We next want to relate the camera output voltage to the incident sensor flux ϕ in lumens and then to some target related parameters. The relationship between sensor output current and incident illumination is given by the responsivity:

$$R(\lambda) = \frac{\text{output camera (sensor) current}}{\text{incident light level input}} \qquad \left(\frac{\mu A}{\ell m}\right)$$

and is a function of the light wavelength λ.

The change in output camera voltage (for a pixel) due to a change in the incident flux $\Delta\phi(\lambda)$ can be expressed as

$$\begin{aligned} \Delta\mu &= R_o \cdot \Delta I_o \\ &= R_o A_i \cdot \Delta I_p \\ &= R_o A_i R(\lambda) \cdot \Delta\phi_p(\lambda) \end{aligned} \tag{16}$$

where R_o is the output load impedance, ΔI_o is the change in the output current, A_i is the current gain of the camera system, and ΔI_p and $\Delta \Phi_p(\lambda)$ are the changes in the output current and input flux, respectively, per pixel.

However, ΔI_p can be related to a change in faceplate illuminance $\Delta E_{fp}(\lambda)$ in lx by:

$$\Delta I_p = A_I R(\lambda) \cdot \Delta E_{fp}(\lambda) \tag{17}$$

where A_I is the total sensor area. Equation (17) is derived in Appendix B.

The faceplate illuminance may be obtained from the following equation [7].

$$E_{fp}(\lambda) = \frac{E_{sc}(\lambda) T_L(\lambda) r(\lambda)}{4F^2} \quad (\ell x) \tag{18}$$

where $E_{sc}(\lambda)$ is the scene illuminance (ℓx), $r(\lambda)$ is the scene reflectance, $T_L(\lambda)$ is the lens transmission factor, and F is the camera lens F-number. A derivation for (18) is given in Appendix C.

Combining (16), (17), and (18) provides an expression for the change in output voltage due to a change in the scene reflectance $\Delta r(\lambda)$:

$$\Delta v = \frac{R_o A_i A_I E_{sc}(\lambda) T_L(\lambda) R(\lambda) \cdot \Delta r(\lambda)}{4F^2} \quad \text{(volts)} \tag{19}$$

Some typical design parameters are given in Table 1 for a camera employing a GE Si-target vidicon. Si-vidicon cameras are low light devices sensitive in both incandescent (tungsten) and infrared light. Substituting these parameters into (19) yields (for constant scene illumination, i.e., $E_{sc}(\lambda)$ = constant for all λ):

$$\Delta v = \frac{(75\Omega)(4.44 \times 10^4)(2.8 \times 10^{-5} m^2)(72 \ell m/m^2)(.9)}{4(2.8)^2} R(\lambda) \cdot \Delta r(\lambda)$$

$$= 192 \ell m\, \Omega \cdot R(\lambda) \cdot \Delta r(\lambda) \tag{20}$$

A normalized plot of $R(\lambda)$ is shown in Figure 7 for an EPICON tube for which the peak value of $R(\lambda)$ is approximately 5200 $\mu A/\ell m$ [11]. Combining this information with (20) allows us to compute the differential voltage $\Delta\mu$ as a function of wavelength and of reflectance changes $\Delta r(\lambda)$. Furthermore $\Delta r(\lambda)$ can be interpreted as a change in the background reflectance due to the presence of an intruder.

Detection performance curves are shown in Figure 8 as a function of $\Delta r(\lambda)$ and for constant scene illumination (72 ℓx) at various wavelengths. These curves were obtained by using (10) and (11) with (20) and represent a lower bound on detection probability.

Reflectance or light level changes due to an intruder in excess of 10% will be detected with a very high probability for the portion of the visible spectrum with wavelengths above 500 nm. The camera's spectral response to violet light (λ = 400 nm) is relatively low but even high detection probabilities can be realized for Δr in excess of 25%. Note that the camera/detector also is sensitive in the near infrared (λ = 900 nm) with correspondingly good detection performance.

The system is not particularly vulnerable to compromise because of its spectral response in both the visible and near infrared light. For interior applications, rooms can be designed to have varying spatial reflectance values so that matching the background would be extremely difficult.

The P_{FA} can be computed from (9) and (14) for δ_i = 62.5 mV. The result using the σ in (15) is below 10^{-10} and corresponds to a false alarm rate (FAR) of less than 1 per year (the P_{FA} and FAR are related by the frame time).

Figure 8 represents a lower bound on P_D where a minimum of two pixel detectors per field are assumed to be involved. Higher P_D's are achieved for corresponding Δr's when additional pixel detectors experience gray contrast changes. This effect is illustrated in Figure 9 for λ = 500 nm and

where n = 2, 3, and 4 pixel sensors per field are involved in the detection process. Equations (12), (13) and (19) were used to obtain Figure 9.

The detection performance is, of course, range critical. In the Telesentry design concept scene widths greater than 280 feet are difficult to protect [7].

Concluding Remarks

We have presented some concepts for quantifying the performance of a class of CCTV-MTI designs employing individual pixel detectors. The concepts should have direct application to other classes of MTI's since the limitations to the detection process usually can be attributed to the camera electronics. Because of this a noise analysis was performed for a generic camera design to better understand the various sources of signal degradation.

We primarily developed a bounding case for the performance of the MTI considered herein; that is, lowest detection probability and highest false alarm rate. Even under these conditions a very high detection probability (~1) was obtained for gray level changes in scene reflectance (e.g., due to an intruder) of less than 12% for the portion of the visible spectrum with wavelengths from 500 nm to 800 nm. The resulting false-alarm rate was less than one per year. Compromising the detection process can be made very difficult because of its sensitivity in the near infrared as well as the visible.

Implicit in the performance calculations was the importance of various design parameters (e.g., sensor responsivity, lens F-number, source illumination and spectral response, etc.). We did not address sources of nuisance alarms due to adverse environments, reliability, resistance to tampering, or even the spatial frequency response of the optics. An optical system which is dirty, damaged, or out-of-focus could certainly degrade performance. All of the above are important and will influence overall system performance.

TABLE 1

TYPICAL DESIGN PARAMETERS

Lens

$T_L(\lambda) = 90\% \quad \forall \quad \lambda$

$F = 2.8$

1/2 inch vidicon

Sensor

$R_{peak} = 5200\ \mu A/\ell m$

$A_I = 0.28\ cm^2$

Camera Electronics

$A_i = 4.44 \times 10^4$

$R_o = 75\Omega$

SNR = 45 dB

Scene Illuminance

E_{sc} = 72 ℓx (maximum possible without sensor saturation at R_{peak})

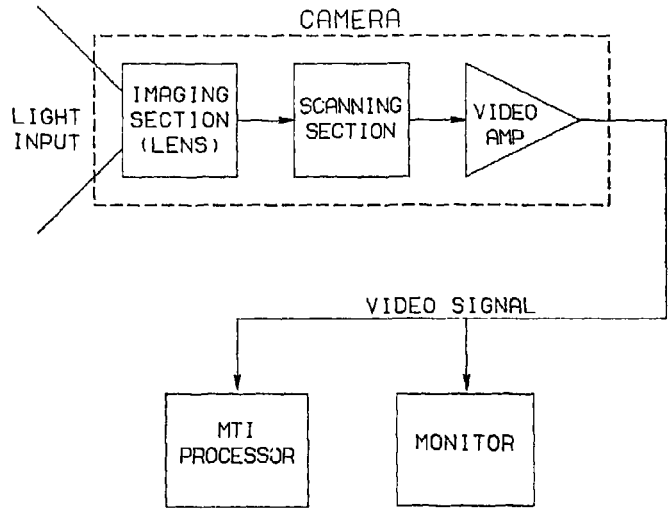

FIGURE 1. BLOCK DIAGRAM OF A CCTV-MTI SYSTEM

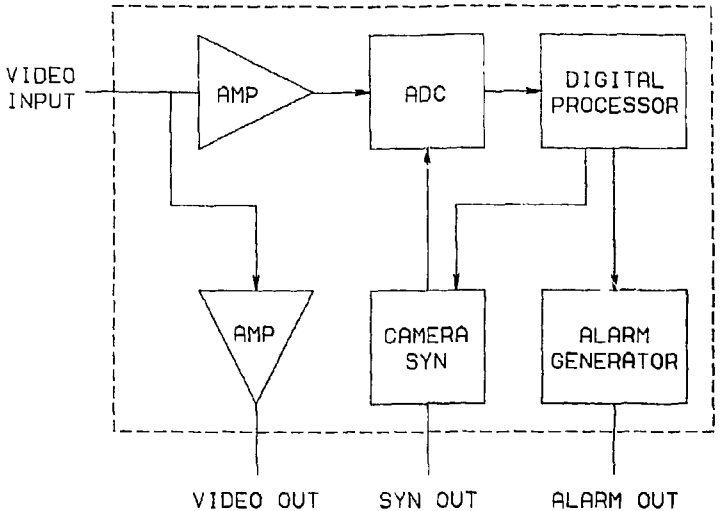

FIGURE 2. SIMPLIFIED BLOCK DIAGRAM OF A MTI PROCESSOR

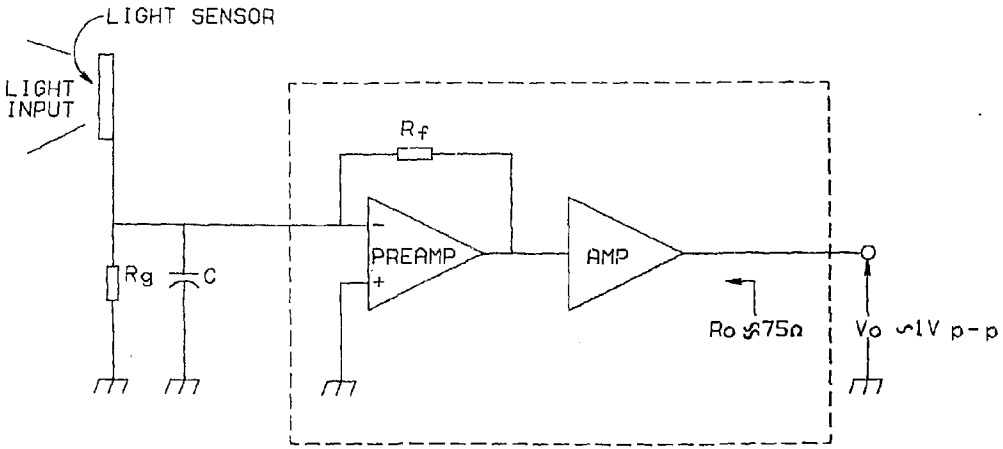

FIGURE 3. CAMERA SIGNAL PATH

FIGURE 4. CAMERA SIGNAL PATH INCLUDING NOISE SOURCES

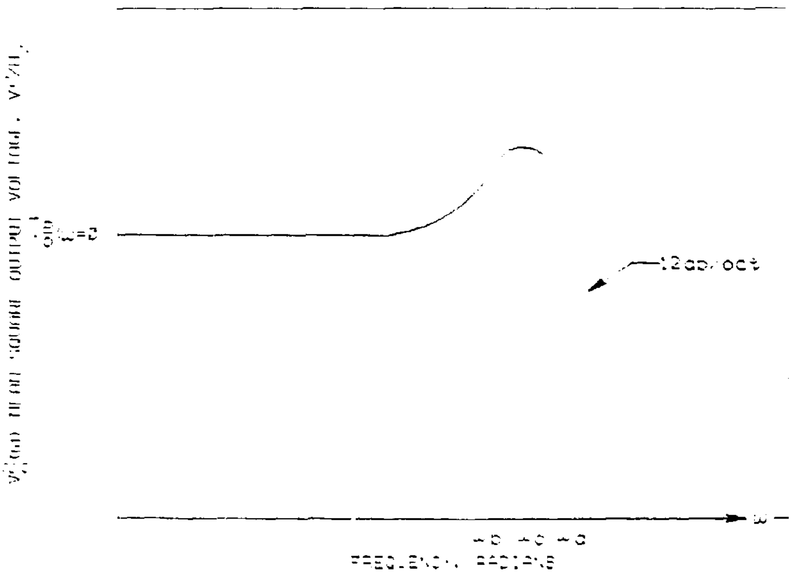

FIGURE 5. OUTPUT NOISE SPECTRUM

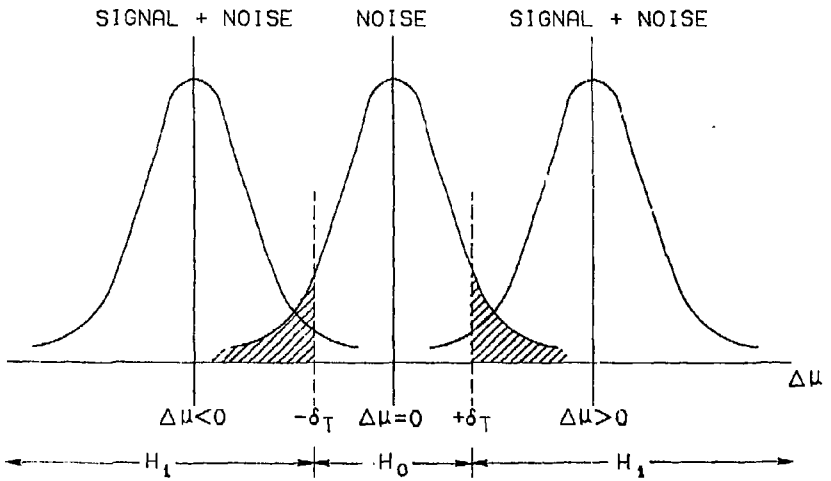

FIGURE 6. THEORETICAL PROBABILITY DENSITY FUNCTIONS FOR SIGNAL AND NOISE.

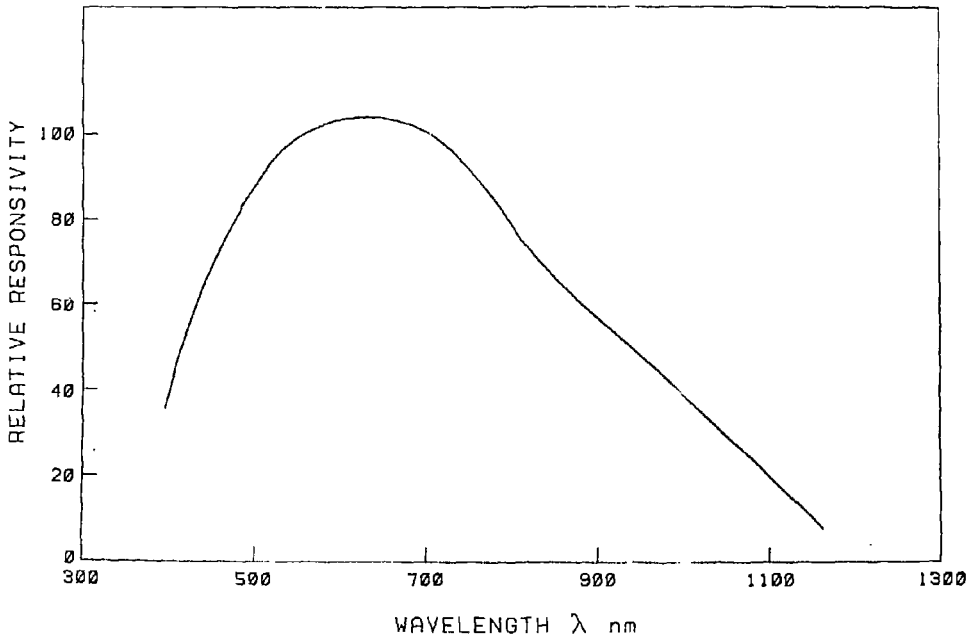

FIGURE 7. RELATIVE RESPONSIVITY AS A FUNCTION OF WAVELENGTH (FOR EQUAL VALUES OF SIGNAL OUTPUT CURRENT AT ALL WAVELENGTHS GE Z-7969S, Z-7960S) [10].

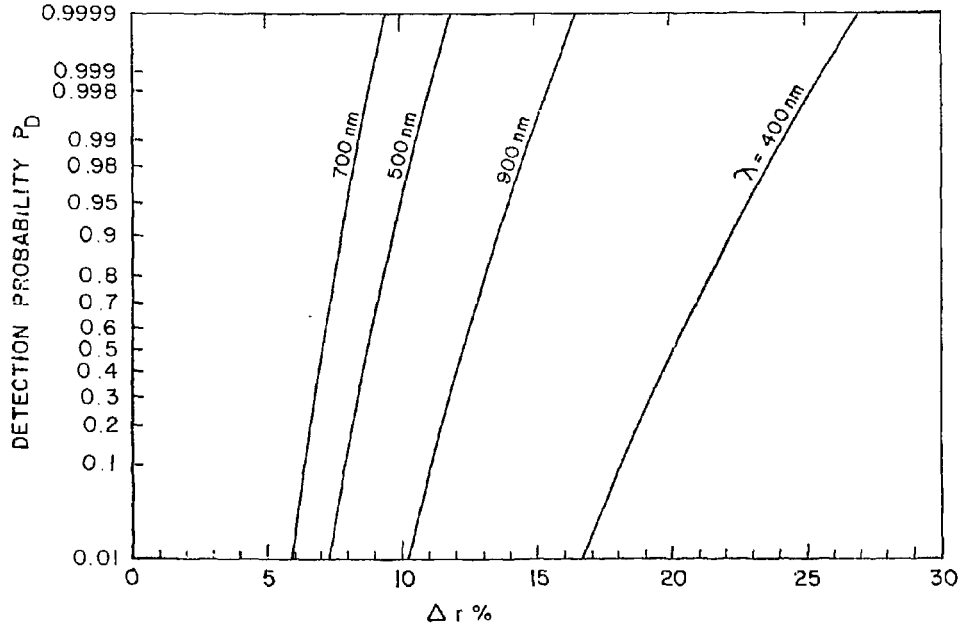

FIGURE 8. DETECTION PERFORMANCE CURVES IN TERMS OF REFLECTANCE CHANGES Δr AND WAVELENGTH λ (SCENE ILLUMINATION EQUALS 72 ℓx FOR ALL λ's)

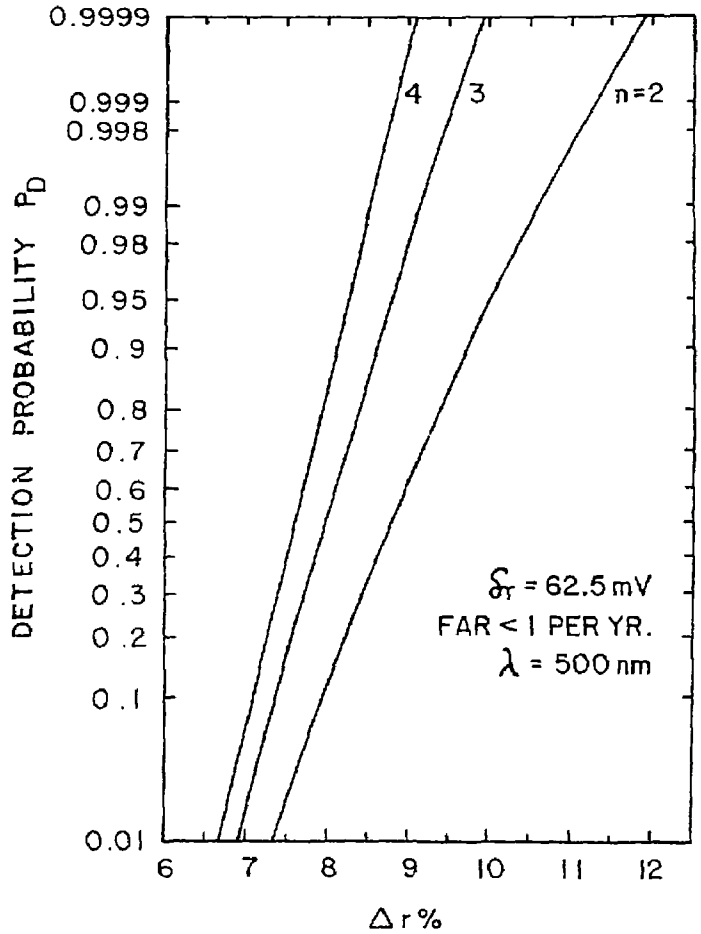

FIGURE 9. DETECTION PERFORMANCE CURVES AS A FUNCTION OF REFLECTANCE CHANGES Δr AND OF THE NUMBER n OF PIXEL DETECTORS ACTIVATED PER FIELD. (SCENE ILLUMINATION EQUALS 72 ℓx λ = 500nm).

REFERENCES

1. Cleland, L. L., et al., Safeguards Material Control at Licensed Processing Facilities, UCID-17525-77-1, Lawrence Livermore Laboratory, Livermore, CA, March 1977.

2. Maimoni, A., et al., Procedure for the Assessment of Material Control and Accounting Systems, UCRL-80814, INMM Meeting, Cincinnati, Ohio, June 27-28, 1978

3. Prell, J. A., Basic Considerations for Assembling a Closed-Circuit Television System, NUREG-0178, U. S. Nuclear Regulatory Commission, May 1977.

4. Prell, J. A., Interior Intrusion Alarm Systems, NUREG-0320, U. S. Nuclear Regulatory Commission, February 1978.

5. M.M.S., Inc., Video Motion Detector, VMD-3001, Torrance, CA.

6. Boyce, Clarence, Private Communication, Information Processing Systems, Belmont, CA, February 1978.

7. Garceau, John, Private Communication, January 1978.

8. Jackson and Church Electronics Company, Melbourne, Florida, Circa 1974.

9. Electro-Optics Handbook, EOH-11, RCA Corporation, 1974.

10. Graeme, J. G., et al., Operational Amplifiers, McGraw-Hill Book Company, San Francisco, CA 1971.

11. General Electric, Technical Literature FPS-EPICON Z-79695, Z-79605, Image and Display Devices Products Section, Syracuse, NY, January 31, 1975.

12. Seyrafi, Khalil, Electro-Optical Systems Analysis, Electro-Optical Research Company, Los Angeles, CA, 1973.

APPENDIX A

In Appendix A we derive the output noise voltage spectrum of the preamplifier circuit in Figure 3 and also show how to obtain the equivalent input current noise. The preamplifier converts the camera tube's output to a voltage and is known as a transimpedance amplifier. Generally there are six sources of noise in such an amplifier: the signal current and dark current shot noise, the source and feedback resistance Johnson noise, and the amplifier's current noise and voltage noise (see Figure 4). The first five noise sources have the same spectrum while the voltage noise has its own unique noise spectrum.

We will first analyze the output noise due to the source resistor, R_g. Then by inspection we can state the results for the remaining noise sources with the exception of $\overline{V}_{ns}^2$ (the preamplifier's series noise contribution) which must be analyzed separately.

Basically what is necssary is to evaluate an integral of the following form.

$$\overline{V}_{ol}^2 = \overline{I}_{ng}^2 \int_0^\infty |H(f)|^2 df \tag{A-1}$$

where H(f) is the preamplifier's spectrum when driven by the source resistor's one-sided white noise spectrum $\overline{I}_{ng}^2$. By use of Figure 4 and after disabling all noise sources except $\overline{I}_{ng}^2$ one obtains the following equation for the output voltage as a function of V_{ng}, the source resistor's noise voltage:

$$V_{ol}(s) = \frac{-K(s)V_{ng}}{R_g\left[\frac{1}{R_g} + \frac{1}{R_f} + Cs + \frac{K(s)}{R_f}\right]} \tag{A-2}$$

where K(s) is the frequency dependent voltage gain of the amplifier, s is the complex frequency variable, and $V_{ng} = I_{ng}R_g$ *in volts/Hz*$^{1/2}$.

Next the bandwidth of the amplifier will be characterized as a single pole so that the gain K(s) can be modeled as

$$K(s) \triangleq \frac{K_d}{s/\omega_a + 1} \tag{A-3}$$

where K_d is the midband voltage gain of the amplifier and ω_a is the 3 db breakpoint. Substituting this gain relationship back into (A-2) results in the following equation (after some algebra):

$$V_{o1}(s) = \frac{\dfrac{-K_d R_f}{R_g+R_f} \dfrac{V_{ng}}{\left(\dfrac{s}{\omega_a}+1\right)\left(\dfrac{s}{\omega_b}+1\right)}}{1+\left(\dfrac{K_d R_f}{R_g+R_f}\right)\left(\dfrac{R_g}{R_f}\right)\left(\dfrac{1}{\dfrac{s}{\omega_a}+1}\right)\left(\dfrac{1}{\dfrac{s}{\omega_b}+1}\right)} \qquad \text{(A-4)}$$

We can recognize the open loop response of this network from (A-4) as:

$$A_1^{O\ell}(s) \triangleq \left(\frac{-K_d R_f}{R_g+R_f}\right)\left(\frac{1}{s/\omega_a+1}\right)\left(\frac{1}{s/\omega_b+1}\right)$$

where $$\omega_b \triangleq \left(\frac{1}{\dfrac{R_f R_g}{R_f+R_g} C}\right) \qquad \text{(A-5)}$$

is a pole caused by the capacitance at the input to the preamplifier.

We have assumed in this analysis that the amplifier pole is larger than the camera tube's input pole. We should point out that for the amplifier to have good stability requires that the gain and phase margins be at least 10 db and 50° respectively. To make the amplifier stable will require some means of adjusting the gain term.

The closed loop gain response $A_1^{C\ell}(s)$ of the preamplifier with respect to V_{ng} can be determined by a rearrangement of (A-4):

$$A_1^{C\ell}(s) \triangleq \left[\frac{-\dfrac{K_d R_f}{R_f+R_g}}{1+\dfrac{K_d R_f}{R_f+R_g}\dfrac{R_g}{R_f}}\right] \frac{1}{1+\left(\dfrac{s}{1+\dfrac{K_d R_g}{R_g+R_f}}\right)\left(\dfrac{1}{\omega_a}+\dfrac{1}{\omega_b}\right)+\dfrac{s^2}{\omega_a\omega_b\left(1+\dfrac{K_d R_g}{R_g+R_f}\right)}} \qquad \text{(A-6)}$$

This equation is composed of two parts, a coefficient term which is not a function of frequency and normalized frequency dependent term. The former will be designated the dc feedback or loop gain and can be expressed as:*

$$A_1^{Cl} \triangleq \frac{-\frac{K_d R_f}{R_f + R_g}}{1 + \left(\frac{K_d R_f}{R_f + R_g}\right)\left(\frac{R_g}{R_f}\right)} = \frac{A_1^{Ol}}{1 + \beta A_1^{Ol}} \qquad (A\text{-}7)$$

where $A_1^{Ol} \triangleq -\frac{K_d R_f}{R_f + R_g}$ is the open-loop gain,

and $\beta \triangleq -\frac{R_g}{R_f}$ is the feedback factor.

When the amplifier's gain K_d becomes large, the equation reduces to the familiar form

$$A_1^{Cl} = -\frac{R_f}{R_g}$$

The frequency dependent term of (A-6) is in the form:

$$H_1(s) \triangleq \frac{1}{1 + 2\rho\frac{s}{\omega_0} + \frac{s^2}{\omega_0^2}}$$

where $\omega_0^2 = \omega_a\omega_b(1 + \beta A_1^{Ol})$ is the natural frequency of the system,

and $\rho = \frac{\omega_a + \omega_b}{2\omega_0}$ is the damping ratio.

Substituting $s = j\omega$ in the above equation for $H_1(s)$ and solving for the magnitude gives the spectrum of the measuring system or preamplifier:

$$|H_1(\omega)|^2 = \left\{\left[1 - \left(\frac{\omega}{\omega_0}\right)^2\right]^2 + 4\rho^2\left(\frac{\omega}{\omega_0}\right)^2\right\}^{-1} \qquad (A\text{-}8)$$

*For convenience we will adopt the following notation:

$A_1^{Ol} \triangleq A_1^{Of}(s)\Big|_{s=0}$ for the open-loop voltage gain and

$A_1^{Cl} \triangleq A_1^{Cf}(s)\Big|_{s=0}$ for the closed-loop voltage gain.

Since the magnitude of (A-8) is unity for $\omega = 0$, we can compute an equivalent noise bandwidth Δf_1 by integrating (A-8) over all positive frequencies. That is

$$\Delta f_1 \triangleq \int_0^\infty \frac{df}{\left[1 - (f/f_o)^2\right]^2 + 4\rho^2(f/f_o)^2} \tag{A-9}$$

where $\omega_o = 2\pi f_o$. Equation (A-9) is in essence the integration denoted in (A-1). Therefore the ouput mean-square noise voltage due to $\overline{I}_{ng}^2$ can be obtained from (A-1), (A-7) and (A-9):

$$\overline{V}_{o1}^2(\overline{I}_{ng}^2) = |A_1^{C\ell}|^2 \overline{V}_{ng}^2 \int_0^\infty |H_1(\omega)|^2 df$$

$$= |A_1^{C\ell}|^2 \overline{V}_{ng}^2 \cdot \Delta f_1$$

$$= |A_1^{C\ell}|^2 R_g^2 \overline{I}_{ng}^2 \cdot \Delta f_1 \tag{A-10}$$

Results will be stated for $\rho = 0.707$ which is representative of a typical design. In this case, the integral in (A-9) evaluates to

$$\Delta f_1 = \frac{\pi}{2\sqrt{2}} f_o \tag{A-11}$$

which is the equivalent noise bandwidth for all the noise sources with the exception of V_{ns}.

By inspection of Figure 4 and from (A-10) and (A-11) we can write the output noise voltage due to all the noise sources besides V_{ns} as:

$$\overline{V}_o^2 = |A_2^{C\ell}|^2 \overline{V}_{01}^2$$

$$= |A_1^{C\ell} A_2^{C\ell}|^2 \left[R_g^2(\overline{I}_{savg}^2 + \overline{I}_D^2 + \overline{I}_{ng}^2 + \overline{I}_{nf}^2 + \overline{I}_{np}^2)\right] \frac{\pi}{2\sqrt{2}} f_o \tag{A-12}$$

where the noise source terms are defined in (1) and $A_2^{C\ell}$ is the second amplifier closed-loop dc voltage gain.

We will now derive the response due to the preamplifier series noise voltage, V_{ns}. Referring to Figure 4, the voltage V_{o1} as function of V_{ns} can be written as:

$$V_{o1}(V_{ns},s) = \frac{-K(s) \cdot \left[\frac{1}{R_g} + \frac{1}{R_f} + Cs\right] V_{ns}}{\left[\frac{1}{R_g} + \frac{1}{R_f} + Cs + \frac{K}{R_f}\right]} \qquad \left(\frac{V}{Hz^{1/2}}\right)$$

Substituting (A-3) for the gain K(s) and reducing the algebra yields

$$V_{o1}(V_{ns},s) = \frac{A_1^{o\ell}\left(\frac{R_f + R_g}{R_f}\right)\left(1 + \frac{s}{\omega_b}\right) V_{ns}}{1 + \frac{s}{1 + \beta A_1^{o\ell}}\left(\frac{1}{\omega_a} + \frac{1}{\omega_b}\right) + \frac{s^2}{\omega_a \omega_b (1 + \beta A_1^{o\ell})}} \qquad \text{(A-13)}$$

The frequency dependent term in this instance becomes

$$|H_2(f)|^2 \triangleq \frac{1 + (f/f_b)^2}{\left[1 - \left(\frac{f}{f_o}\right)^2\right]^2 + 4\rho^2\left(\frac{f}{f_o}\right)^2} \qquad \text{(A-14)}$$

and the equivalent bandwidth is

$$\Delta f_2 = \int_0^\infty \frac{1 + (f/f_b)^2 \, df}{\left[1 - \left(\frac{f}{f_o}\right)^2\right]^2 + 4\rho^2\left(\frac{f}{f_o}\right)^2} \qquad \text{(A-15)}$$

Evaluating (A-15) for the case of $\rho^2 = 1/2$ yields

$$\Delta f_2 = \frac{\pi}{2\sqrt{2}} f_o \left[1 + (f_o/f_b)^2\right] \qquad \text{(A-16)}$$

The mean-square output voltage due to $\overline{V}_{ns}^2$ can be obtained from (A-13) and (A-16) and is

$$\overline{V}_o^2(\overline{V}_{ns}^2) = |A_2^{c\ell}|^2 \, \overline{V}_{o1}^2$$

$$= |A_1^{c\ell} A_2^{c\ell}|^2 \left[\frac{R_f + R_g}{R_f}\right]^2 \overline{V}_{ns}^2 \int_0^\infty |H_2(\omega)|^2 df$$

$$= A_1^{c\ell} A_2^{c\ell\ 2} \left[\frac{R_f + R_g}{R_f}\right]^2 \overline{V}_{ns}^2 \, \Delta f_2$$

$$= |A_1^{cl} A_2^{cl}|^2 \left[\frac{R_f + R_g}{R_f}\right]^2 \left[\frac{\pi}{2\sqrt{2}} f_o\right]\left[1 + (f_o/f_b)^2\right]\overline{V}_{ns}^2$$

$$\approx |A_1^{cl} A_2^{cl}|^2 \left[\frac{\pi}{2\sqrt{2}} f_o^3\right]\left[2\pi R_g C\right]^2 \overline{V}_{ns}^2$$

$$\approx |A_1^{cl} A_2^{cl}|^2 \left[\frac{\pi}{2\sqrt{2}} f_o\right]\left[R_g/R_{eq}\right]^2 \overline{V}_{ns}^2 \qquad \text{(A-17)}$$

where use was made of (A-5), and

$$R_{eq} \triangleq \frac{1}{2\pi C f_o} ,$$

and where we note that because f_o is typically much greater than f_b for systems designed with $\omega_a = 2\omega_b(1 + \beta A_1^{ol})$, we can make the approximation that $\Delta f_2 \approx \Delta f_1$. Another possible design is for $\omega_a \approx o$, and in this case an expression different than (A-17) would result.

The total output mean-square noise voltage due to all sources is a summation of (A-12) and (A-17)

$$\overline{V}_o^2 = \frac{\pi}{2\sqrt{2}} f_o \, |A_1^{cl} A_2^{cl}|^2 \left\{R_g^2(\overline{I}_{sig}^2 + \overline{I}_D^2 + \overline{I}_{ng}^2 + \overline{I}_{np}^2 + \overline{I}_{nf}^2 + \frac{1}{R_{eq}^2}\overline{V}_{ns}^2)\right\} \qquad (V^2) \qquad \text{(A-18)}$$

Equation (A-18) gives the variance of the output noise voltage. The variance is also denoted σ_s^2.

The equivalent input noise current $\overline{I}_{in}^2$ can be obtained from (A-18) by noting that

$$\overline{I}_{in}^2 = \frac{\overline{V}_o^2}{|A_1^{cl} A_2^{cl}|^2 R_g^2} \qquad \text{(A-19)}$$

APPENDIX B

The purpose of this appendix is to derive the basis for equation (17). The current from the sensor (irradiated image) is given by

$$I_I \triangleq e\frac{dn}{dt} = R(\lambda)E_{fp}(\lambda)A_I \tag{B-1}$$

where n is the number of electrons, e is the charge on an electron, A_I is the total sensor area, $R(\lambda)$ is the sensor responsivity ($\mu A/\mu m$) and $E_{fp}(\lambda)$ is the faceplate illumination (μx).

Integrating (B-1) with respect to time yields the total number of electrons on the photocathode or sensor surface in a frame time T_F:

$$n = \frac{1}{e}\ R(\lambda)E_{fp}(\lambda)A_I T_F \tag{B-2}$$

The sensor area A_I can be expressed as

$$A_I = pA_p \tag{B-3}$$

where A_p is the area of one pixel and p is the total number of active pixels:

$$p = \left(\frac{\text{number of sample elements}}{\text{line}}\right)\left(\frac{\text{number of lines}}{\text{image}}\right)$$

Using (B-3) in (B-2) we can solve for the total number of electrons per pixel in a frame time:

$$n_p \triangleq \frac{n}{p} = \frac{1}{e}R(\lambda)E_{fp}(\lambda)A_p T_F \tag{B-4}$$

The pixel current I_p therefore can be written as

$$I_p \triangleq \frac{en_p}{T_s} = \frac{A_p T_F}{T_s}\ R(\lambda)E_{fp}(\lambda) \tag{B-5}$$

where T_s is the sampling or readout time per pixel. However,

$$T_F = pT_s \tag{B-6}$$

Therefore, using (B-3) and (B-6) in (B-5) yields

$$I_p = A_I R(\lambda)E_{fp}(\lambda) \tag{B-7}$$

which is equation (17). The conclusion is that the total photocathode area can be used to calculate the pixel current.

APPENDIX C

The following analysis calculates the flux density from a lens assembly. Assume the following diagram as the model for a lens system:

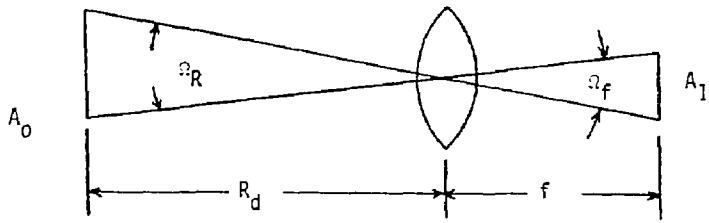

where A_o is the area of the object

A_I is the area of the image or sensor target

R_d is the range or distance from object to lens

f is the focal length of the lens

Ω_R is the solid angle from lens to object

Ω_f is the solid angle from lens to image

In a lens system $\Omega_R = \Omega_f$ so that the following is true

$$\frac{A_o}{R_d^2} = \frac{A_I}{f^2} \quad . \tag{C-1}$$

The flux or power out of the lens must be

$$\Phi_{out} = T_L \Phi_{in} \qquad (\mu m) \tag{C-2}$$

where:

Φ_{in} is the input power to the lens,

T_L is the transmission through the lens,

and Φ_{out} is the output power from the lens.

Power into the lens depends upon the solid angle that the lens makes with the object and is given by the following equation

$$\Phi_{in} = L_o A_o \left(\frac{A_L}{R_d^2}\right) \qquad (\mu m) \tag{C-3}$$

where L_o is the radiance of the object $\left(\frac{\text{ℓm}}{\text{sr m}^2}\right)$,

A_L is the area of the lens (m^2),

and A_L/R_d^2 is the solid angle from object to lens (sr).

Combining equations (C-1) through (C-3) yields

$$\Phi_{out} = L_o \frac{T_L}{f^2} A_I A_L \qquad (\text{ℓm}) \quad .$$

However,

$$\frac{A_L}{f^2} = \frac{\pi}{4}\left(\frac{d}{f}\right)^2 = \frac{\pi}{4F^2}$$

where d is the diameter of the lens and F = (f/d) is called the F-number of the lens. Therefore the output power can be expressed as

$$\Phi_{out} = \frac{\pi L_o T_L A_I}{4F^2} \qquad (\text{ℓm}) \quad .$$

The output flux density at the image plane or sensor faceplate is given by:

$$E_{fp} \triangleq \Phi_{out}/A_I$$

$$= \frac{\pi L_o T_L}{4F^2} \qquad (\text{ℓx}) \quad . \qquad \text{(C-4)}$$

Now assume that the object is irradiated by a source E_{sc} ($\text{ℓm}/m^2$) which has some spectral density. Then the output radiant spectral density is

$$L_o(\lambda) = \frac{1}{\pi} E_{sc}(\lambda) r(\lambda)$$

where $r(\lambda)$ is the reflection coefficient of the object. Substituting this into the equation for the image irradiance (C-4) one obtains the following

$$E_{fp}(\lambda) = \frac{T_L(\lambda) E_{sc}(\lambda) r(\lambda)}{4F^2} \qquad (\text{ℓx}) \quad . \qquad \text{(C-5)}$$

This is the same as equation (18) for the irradiance at the image plane given the source irradiance and object spectral reflection coefficient.